RSC Advances

PAPER

View Article Online
View Journal | View Issue

Cite this: *RSC Adv.*, 2017, **7**, 23787

Boosting visible light photo-/Fenton-catalytic synergetic activity of $BiOIO_3$ by coupling with Fe_2O_3†

Hehua Zeng,*[a] Xiu Liu,[a] Ting Wei,[a] Xueqin Li,[a] Tianxiang Liu,[a] Xuemei Min,[a] Qiuhui Zhu,[a] Xiufeng Zhao[a] and Jianhui Li *[ab]

Received 7th March 2017
Accepted 19th April 2017

DOI: 10.1039/c7ra02761c

rsc.li/rsc-advances

The combination of a semiconductor photocatalyst with guest transition metal oxides can extend its light absorption property in the visible region, leading to the emergence of potential catalysts for solar photocatalytic degradation. In the present study, $Fe_2O_3/BiOIO_3$ nanosheets with heterojunction couples have been fabricated in one-step by a simple hydrothermal method and used as a heterogeneous Fenton-like photocatalyst for the oxidative degradation of *p*-nitrophenol (PNP) under visible light. The absorption range of $BiOIO_3$ extended to the visible light region with the introduction of Fe, while the band gap is dramatically decreased from 3.00 eV for pure $BiOIO_3$ to 1.81 eV for 30% $Fe_2O_3/BiOIO_3$. The recombination of photogenerated electron–hole pairs can also be prevented effectively. The intrinsic relationship between structure and catalytic activity was fully studied and a possible catalytic mechanism was proposed. The enhanced photocatalytic activity can be attributed to the synergistic effect of heterojunction semiconductor photocatalysis and heterogeneous Fenton catalysis caused by $BiOIO_3$ and Fe_2O_3. This highly active heterogeneous catalyst has the potential for efficient utilization of solar energy in the visible range and can be applied in environmental remediation and waste water treatment.

1. The introduction

Semiconductor photocatalysis, based on the promotion of redox reactions by photoexcited electrons and holes under light irradiation, is a green technique that can be used for the oxidation of organic pollutants into CO_2 and H_2O without secondary pollution. In the past several years, bismuth-based layered photocatalysts, such as Bi_2S_3,[1] Bi_2WO_6,[2] BiOX (X = Cl, Br, I),[3–8] and $BiIO_4$,[9] have been a hot area of research because of their special structure that can effectively separate photogenerated carriers. Recently, nanostructured $BiOIO_3$ possessing two lone-pair cations and displaying an Aurivillius-type $(BiO)_2^{2+}$ layer has been reported to exhibit high photocatalytic activity.[10–12] However, it can only be excited by ultraviolet light that occupies only about 5% of the solar light due to its wide bandgap, which restricts the practical applications. Therefore, further researches for the broadening of the absorption spectrum of $BiOIO_3$ have been carried out, including the synthesis of $BiOIO_3$/g-C_3N_4,[13] Bi/I^-/$BiOIO_3$,[14] Ag/AgCl/$BiOIO_3$ [15] and $BiOIO_3$/BiOI.[16] Nonetheless, the photocatalytic activity of $BiOIO_3$ is far from efficient for practical applications.

Modification using transition metals to the bismuth-based photocatalysts may also be a good way to obtain the enhanced semiconductor photocatalytic activity. The studies on Mn decorated BiOCl and Fe decorated BiOBr have indicated that the doping of transition metals can reduce the band gap of bismuth oxyhalides and extend the wavelength response toward the visible range.[17,18] Therefore, it is believed that $BiOIO_3$ heterojunctions with transition metal oxides can be constructed to increase the response to visible light as well as the photocatalytic activity.

Fenton reagent, which can rapidly convert hydrogen peroxide (H_2O_2) into a stoichiometric amount of hydroxyl free radical (·OH) with high oxidative ability in acidic medium between pH 2 and pH 4, is known for more than a century and considerable as a successful treatment for advanced oxidation process (AOP).[19] Conventional homogeneous Fenton process occurrs in Fe^{2+}/H_2O_2 aqueous system, in which organic pollutants are oxidized by the ·OH produced from H_2O_2 decomposition catalyzed by Fe^{2+}. However, its applications are limited due to the generation of excessive amounts of ferric hydroxide sludge that requires additional separation process. Heterogeneous Fenton-like system employing solid catalyst, which could provide a promising alternative for producing a large amount of hydroxyl free radical, may be available over a wide pH range and prevent ferric hydroxide sludge effectively.[20] Recent years, many

[a]*Department of Chemistry and Applied Chemistry, Changji University, Changji 831100, Xinjiang, China. E-mail: hhzeng@cjc.edu.cn*

[b]*National Engineering Laboratory for Green Chemical Productions of Alcohols–Ethers–Esters, College of Chemistry and Chemical Engineering, Xiamen University, Xiamen 361005, Fujian, China. E-mail: jhli@xmu.edu.cn*

† Electronic supplementary information (ESI) available. See DOI: 10.1039/c7ra02761c

heterogeneous catalysts such as zero-valent iron,[21,22] iron oxides[23,24] and other iron-containing materials[19,20,25,26] have been studied. Fe_2O_3, the most stable iron oxide under ambient conditions, is widely used in catalysts and water treatment. The band gap energy of Fe_2O_3 is 2.2 eV, and can be activated with visible light (<560 nm). In recent years, the combination of Fe_2O_3 and different nanospecies for photocatalytic reactions has received much attention.[27–29]

Herein, a novel $BiOIO_3$ nanosheets married with various doping level of Fe_2O_3 were constructed in a one-pot route by the facile hydrothermal method. The binary photocatalysts were employed as heterogeneous catalyst to oxidize *p*-nitrophenol (PNP) in the presence of H_2O_2. The trapping experiment and photoluminescence probing technique were used to verify the active species of photocatalytic process. The effect of initial parameters on the oxidation of PNP was investigated in detail, and the catalytic mechanism was also preliminarily studied.

2. Materials and methods

2.1 Reagents

All the reagents were of analytical grade and used without further purification. Potassium iodate (KIO_3), iron nitrate ($Fe(NO_3)_3\cdot 9H_2O$), bismuth nitrate ($Bi(NO_3)_3\cdot 5H_2O$) were provided by Sinopharm Chemical Reagent Beijing Co., Ltd. PNP and hydrogen peroxide (H_2O_2, 30 wt%) was supplied by Beijing Chemical Factory. The other reagents were analytically pure, ultrapure water was used throughout the study.

2.2 Preparation and characterization of catalysts

Firstly, 1 mmol of $Bi(NO_3)_3\cdot 5H_2O$ was dispersed in 20 mL deionized water by ultrasonic method to form solution A. Simultaneously, 1 mmol KIO_3 was fully dissolved in 20 mL deionizer water to form solution B. Then the solution B was dropped into the solution A. After magnetic stirring for 30 min, a certain amount of NaOH solution was added to adjust the pH value of the precursor to 3. Then, another 20 mL water solution containing a stoichiometric $Fe(NO_3)_3\cdot 9H_2O$ was dropped into the above suspension under the magnetic stirring condition, the concentration of Fe ions was chosen as 5%, 10%, 15%, 20%, 25%, and 30% (Fe_2O_3 and $BiOIO_3$ in the mass percent). The mixture was transferred into a 100 mL Teflon-lined stainless autoclave to perform hydrothermal process at 180 °C for 12 h and allowed to cool down to room temperature naturally. The precipitate was washed using distilled water and absolute ethanol for three times and then dried at 80 °C for 12 h. The obtained samples were named as *x*% $Fe_2O_3/BiOIO_3$, where *x* represents the percent concentration of Fe_2O_3.

Fourier transform infrared spectrometry (FT-IR, IR Affinity-1), UV-vis diffuse reflection spectrometry (UV-vis DRS, UV-2550), X-ray powder diffraction (XRD, XD-2 Cu Kα radiation), field emission scanning electron microscopy (FE-SEM, 55VP SUPRA), transmission electron microscopy (TEM, JEOL JSM-2010), X-ray photoelectron spectrometer (XPS, ESCALAB MK II), and fluorescence spectrophotometer (PL, RF-5301) were performed to characterize the resultant catalysts.

2.3 Photocatalytic evaluation

The photocatalytic activities of the products were evaluated by degradation of PNP at room temperature. The reaction was performed in a photochemical reactor (BL-GHX-V, Shanghai Bilon Instruments Co., Ltd, China), equipped with a 250 W metal halide lamp combined with a 400 nm cut-off filter as light source. In a typical experiment, 50 mg catalyst was dispersed into 100 mL of 25 mg L^{-1} PNP solution with magnetic stirring to maintain a uniform suspension. The initial pH of the suspension was adjusted to a certain value using dilute aqueous H_2SO_4 or NaOH solution. After 30 min of stirring in the dark to reach the adsorption/desorption equilibrium, the reaction was timed with addition of H_2O_2 solution. At given time intervals, 5 mL of the suspension was continually collected. The solution and the catalyst were separated by centrifuging and the concentration of the remaining PNP was determined at 316 nm using a UV/Vis spectrophotometer. Total organic carbon (TOC) was obtained by a TOC analyzer (Shimadzu TOC-V CPH). Experiments were carried out in triplicate, and the results were expressed as mean values.

3. Results and discussion

3.1 Textural and structural properties

The crystal quality of the as-synthesized samples was analyzed by X-ray diffraction (XRD) as showed in Fig. 1. All patterns of samples exhibit sharp diffraction peaks, indicating that all samples were highly crystalline. It can be seen that $BiOIO_3$ exhibits an orthorhombic crystal structure according to data files (ICSD #262019). With increasing Fe ions concentration, the intensity of (121) peak of $BiOIO_3$ gradually decreased, while the peaks of Fe_2O_3 phase were simultaneously enhanced, which suggesting that the formation of $Fe_2O_3/BiOIO_3$ composites.

The FT-IR spectra are presented in Fig. S1.† All the modified samples possess similar FT-IR spectra to $BiOIO_3$. But the absorption at 516 cm^{-1} becomes weaker upon introduction of Fe_2O_3 with little change in the peak shape and peak position. Meanwhile there is an obvious new absorption peak at 480 cm^{-1} due to Fe–O vibrations of Fe_2O_3.[28] The new weak absorption peak (889 cm^{-1}) could be associated with the stretching

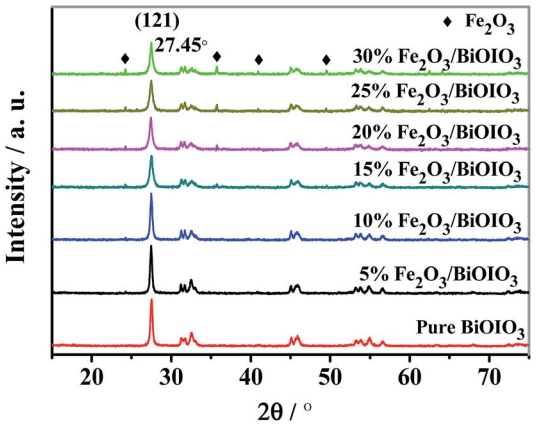

Fig. 1 XRD patterns of pure $BiOIO_3$ and *x*% $Fe_2O_3/BiOIO_3$.

vibration of the Bi–O–Fe bond formed by interactions of $BiOIO_3$ and Fe_2O_3. These results combined with the XRD characterizations further corroborates that Fe_2O_3 has been successfully combined with $BiOIO_3$.

The surface composition and chemical states of related elements of 15% $Fe_2O_3/BiOIO_3$ were analyzed by XPS. The shift of peak position on the charge effect was calibrated using the binding energy of C 1s at 284.6 eV.[30] Fig. 2a shows the survey spectra and Fig. 2b–e shows high-resolution XPS spectra of the four primary elements. Clearly, the peak at 529.7 (Fig. 2b) corresponds to O 1s, which is related to the Bi–O bond in $BiOIO_3$ lattice. Two strong peaks with binding energies at 634.9 and 623.4 eV are observed in the I 3d high-resolution XPS spectrum (Fig. 2c), which are separately attributed to the I^{5+} $3d_{3/2}$, and I^{5+} $3d_{5/2}$. The Bi 4f XPS spectra are shown in Fig. 2d, revealing Bi $4f_{5/2}$ and Bi $4f_{7/2}$ characteristic peaks at 164.5 and 159.0 eV, respectively. The peaks located at 711.5 and 724.8 eV can be assigned to Fe $2p_{3/2}$ and Fe $2p_{1/2}$ (Fig. 2e), respectively, which are in agreement with the value reported for Fe_2O_3.[28]

SEM and TEM revealed the morphologies of the as-prepared samples. Apparently, the sample exhibits irregular thin nanosheets with several hundred nanometers in size (Fig. 3a and b). The HRTEM image shown in Fig. 3c further verified the presence of Fe_2O_3. The lattice spacing of pure $BiOIO_3$ is 0.289 nm, corresponding well to the (002) plane of the orthorhombic $BiOIO_3$.[23] Another distinct lattice fringe with a spacing of 0.368 nm was found on the edge of the $Fe_2O_3/BiOIO_3$ flake, this lattice spacing matches well with the (012) plane of Fe_2O_3. EDX mapping was conducted to inspect the elemental composition and distribution (Fig. 3d–g). It is obvious that there is a homogeneous distribution of Fe, Bi, O and I elements in 15% $Fe_2O_3/BiOIO_3$. These results above showed successful formation of $Fe_2O_3/BiOIO_3$ heterojunction.

The optical properties of the as-prepared samples were measured by a UV-Vis spectrometer. As can be seen in Fig. S2a,† $BiOIO_3$ has a clear edge around 400 nm without obvious absorption in the visible-light region. After $Fe_2O_3/BiOIO_3$ heterojunction is formed, the optical absorption exhibits a systematical red shift with a wide and strong light absorption in the visible light range. The corresponding $h\nu = (Ah\nu)^{1/2}$ plot for the samples are shown in Fig. S2b.† The band gaps were estimated to be about 3.00 eV and 1.81 eV for pure $BiOIO_3$ and 30% $Fe_2O_3/BiOIO_3$ by the linear extrapolation, respectively.

The photoluminescence (PL) emission spectra is usually employed to investigate the migration, transfer and recombination processes of photogenerated charge carriers in semiconductors, which plays a crucial role in photocatalytic reaction. Generally, the lower PL intensity, the lower recombination rate of photogenerated electron–hole pairs, thus there are more oxidative species and higher photocatalytic activity. Fig. 4 exhibits the PL spectra of the as-prepared samples under the excitation wavelength of 300 nm, and all the PL spectra exhibit similar peak shape and peak position. Obviously, the PL intensity of various $Fe_2O_3/BiOIO_3$ samples is lower than that of pure $BiOIO_3$, indicating that the recombination of photogenerated electron–hole pairs can be efficiently prevented by the introduction of Fe_2O_3. The 15% $Fe_2O_3/BiOIO_3$ sample possesses the lowest PL intensity, suggesting the highest separation efficiency of photogenerated electrons and holes. However, when Fe_2O_3 concentration further increased, the PL emission intensity of samples increased, leading to inferior separation of the electron–hole pairs.

3.2 Photocatalytic performance

The effects of various reaction parameters on the oxidation of *p*-nitrophenol are presented in Fig. 5. Except for the investigated

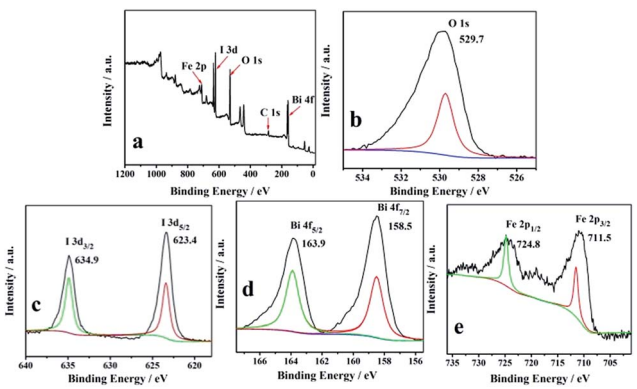

Fig. 2 XPS spectra of the 15% $Fe_2O_3/BiOIO_3$ sample: (a) a wide-scan spectrum, the spectra in the energy regions of (b) O 1s, (c) I 3d, (d) Bi 4f, and (e) Fe 2p states.

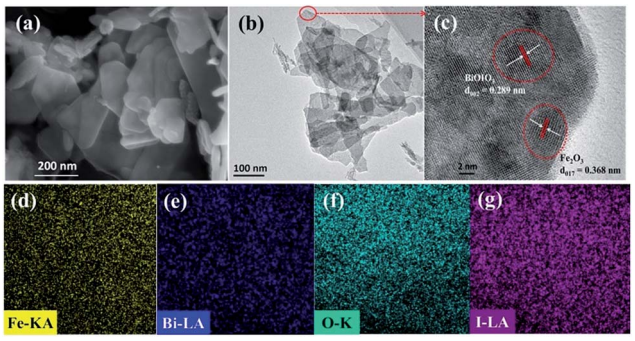

Fig. 3 (a) SEM image, (b–c) TEM image, (d–g) EDX mapping of 15% $Fe_2O_3/BiOIO_3$.

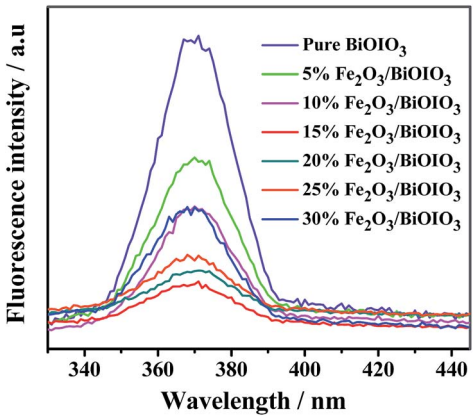

Fig. 4 PL spectra of pure $BiOIO_3$ and *x*% $Fe_2O_3/BiOIO_3$.

parameter, others are fixed on the following conditions: irradiation (λ > 400 nm), PNP 25 mg L^{-1}, H_2O_2 0.204 g L^{-1}, 15% $Fe_2O_3/BiOIO_3$ 0.5 g L^{-1}, pH 6.5 and room temperature. From the results, it is clear that all x% $Fe_2O_3/BiOIO_3$ samples exhibit much higher oxidation ability for PNP than pure $BiOIO_3$ (Fig. 5a). Among these samples, 15% $Fe_2O_3/BiOIO_3$ sample possesses the highest oxidation ability toward PNP, which is 4 times than that of pure $BiOIO_3$. Excessive amounts of Fe over the catalysts with higher Fe_2O_3 concentration may act as recombination centers for photogenerated carriers and decrease the photocatalytic performance, which is consistent with the PL spectra results in Fig. 4.

H_2O_2 is the source of ·OH, which is regarded as the main oxidative species to degrade organics in photocatalytic process. The influence of initial concentration of H_2O_2 on the degradation is presented in Fig. 5b. The result shows that when H_2O_2 concentration increased from 0 to 0.204 g L^{-1}, the degradation of PNP is remarkably enhanced. Nevertheless, the increase of degradation rate becomes less significant when the concentration of H_2O_2 further increased to 0.272 g L^{-1}. This could be attributed to the scavenging of ·OH which occurred through the following reaction:[31,32]

$$H_2O_2 + \cdot OH \rightarrow H_2O + HO_2\cdot/O_2^{-}\cdot$$

They ($HO_2\cdot/O_2^{-}\cdot$) are much less reactive.[33] Therefore, the optimum H_2O_2 concentration appeared to be around 0.204 g L^{-1} under the conditions used in this study.

As shown in Fig. 5c, the degradation of PNP became very slow under alkaline conditions with pH value of 9.0. Moreover, the degradation efficiency increased significantly with lowering pH value. This increased degradation efficiency can be ascribed to the higher oxidation potential of ·OH and the higher stability of H_2O_2 that cannot decompose immediately to H_2O and O_2 at a lower pH.[20,34] However, under strong acidic condition (pH ≤ 3.0), homogeneous Fenton reaction, which was caused by the releasing of iron ions, could shorten the life of catalyst.

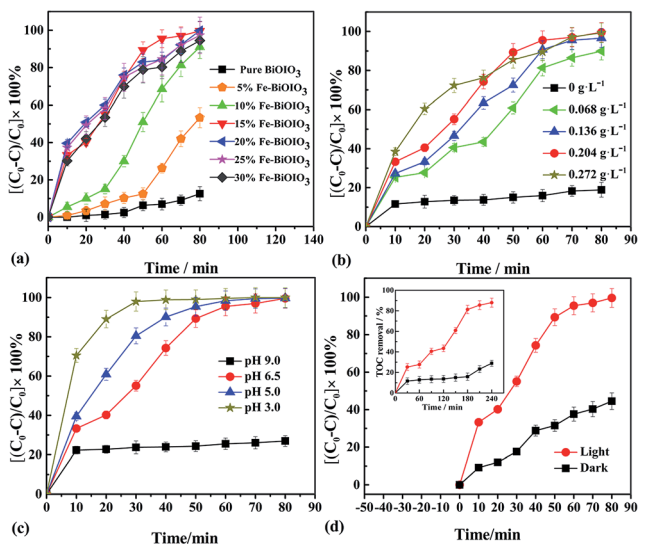

Fig. 5 Influence of (a) introduction of Fe ions, (b) H_2O_2 concentration, (c) pH, and (d) irradiation over the 15% $Fe_2O_3/BiOIO_3$. Except for the investigated parameter, others fixed at [PNP] = 25 mg L^{-1}, [H_2O_2] = 0.204 g L^{-1}, catalyst dosage = 0.5 g L^{-1}, pH 6.5, under irradiation (λ > 400 nm).

The catalytic activity of catalyst was significantly enhanced under irradiation condition compared with that in dark, as showed in Fig. 5d. The degradation efficiency reached to 99.9% after 80 min under irradiation, while it was only 45% in the dark under the same conditions. The similar feature can be observed in TOC removal processes (inset in Fig. 5d). This is a further proof that the synergistic effect of photocatalysis and Fenton-like catalysis of catalyst would be responsible for the degradation of PNP.

The effect of catalyst dosage on degradation of PNP is illustrated in Fig. S3.† The result indicates that higher degradation efficiency was achieved when the catalyst dosage increased from 0 to 0.5 g L^{-1}. However, less obvious change was observed when catalyst dosage was further increased to 1.0 g L^{-1}, which could be ascribed to the agglomeration of particles which led to decline of surface area.[35]

Fig. S4† shows the absorption variation of PNP on the 15% $Fe_2O_3/BiOIO_3$ system, the peak at 316 nm decreased gradually as the irradiation time increased, indicating the destruction of the conjugated structure of the PNP.

3.3 Stability and reusability of the catalyst

It is important to evaluate the stability and reusability of catalyst for practical application of a heterogeneous catalytic system. Therefore, leaching test was determined by ICP-AES by measuring the amount of iron leached into the solution after a reaction time of 80 min. The result shows that only 0.0072 mg L^{-1} of Fe^{3+} leached into the solution for the 15% $Fe_2O_3/BiOIO_3$ sample. A homogeneous Fenton reaction was carried out using the same concentration of Fe^{3+} (prepared from $Fe(NO_3)_3\cdot 9H_2O$) under the same operating conditions. Interestingly, there was not obvious degradation of PNP observed during the catalytic process. Thus, homogeneous contribution of leached Fe^{3+} to degradation of PNP can be ignored. Meanwhile, the reusability was investigated during five consecutive cycles under irradiation and fixed reaction time of 80 min. The degradation efficiency of the reused catalyst was still close to fresh catalyst, as showed in Fig. S5a.† Additionally, the XRD pattern of the catalyst after five times reuse is also shown in Fig. S5b.† No obvious differences in the diffraction peaks was observed, confirming a very stable crystal structure. These results indicate that the as-prepared catalysts exhibit high stability and reusability as a photocatalyst in the AOP process.

3.4 Analysis of the active species

To verify the active species of photocatalytic process, the effect of photogenerated holes (h^+), superoxide radical ($\cdot O_2^-$) and hydroxyl radical (·OH) on the degradation of PNP was investigated. Triethanolamine (TEA), *p*-benzoquinone (BQ) and isopropyl alcohol (IPA) were served as the scavengers of h^+, $\cdot O_2^-$, and ·OH, respectively. After being trapped, the active species

will be efficiently quenched, and the degradation efficiency of PNP thus became lower. As shown in Fig. 6, the addition of IPA resulted in a remarkable decrease in the degradation of PNP, indicating that ·OH is the main active species in the photocatalytic process. Only slight decrease in the degradation efficiency was observed in the presence of TEA and BQ, revealing that h^+, and $\cdot O_2^-$ made negligible contribution to the photocatalytic reaction.

The formation of ·OH on the surface of catalysts was further confirmed by PL technique using coumarin as probe molecule. Coumarin can be rapidly oxidized by photogenerated ·OH in the presence of Fe_2O_3/$BiOIO_3$ and H_2O_2 under irradiation to form hydroxycoumarin, which shows high fluorescence intensity. As illustrated in Fig. S6,† the PL intensity was enhanced rapidly as the reaction time increases. In other words, coumarin can be rapidly oxidized to form hydroxycoumarin by the synergistic effect of irradiation and Fenton catalyst and the PL intensity was increased significantly with reaction time (inset curve 1), which was much higher than that in the dark (inset curve 2). However, the PL intensity was very low under the conditions when single catalyst or H_2O_2 was used (inset curves 3 and 4). On the other hand, the fluorescence for the hydroxycoumarin was completely quenched (inset curve 5) once IPA was added to the system, meaning that ·OH is the principle oxidative species that participate in the heterogeneous Fenton-like photocatalytic reaction.

3.5 Possible photocatalytic mechanism

It is generally believed that the photocatalytic activity can be affected by many factors, which cooperate with each other to determine the photocatalytic activity. The reasons for the enhanced catalytic activities of Fe_2O_3/$BiOIO_3$ samples was explained as follows.

Firstly, in the photocatalytic process, iron ion of the x% Fe_2O_3/$BiOIO_3$ samples can serve as a mediator of the interfacial charge transfer, which can trap photogenerated electrons and holes to form corresponding Fe^{II} and Fe^{IV}.[36] Once Fe^{II} and Fe^{IV} contact with O_2 or OH^- in the solution, they will re-transfer into Fe^{III} together with the formation of $\cdot O_2^-$ or ·OH.[37] Secondly,

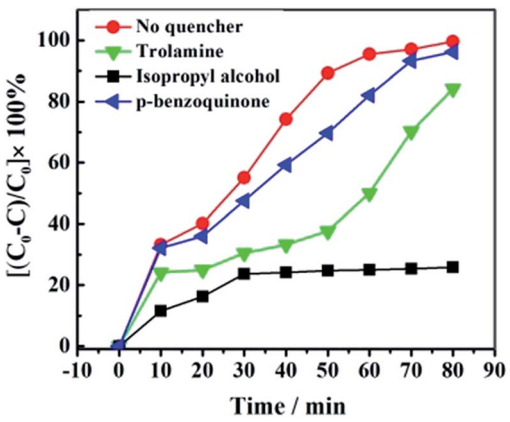

Fig. 6 Active specie trapping experiments.

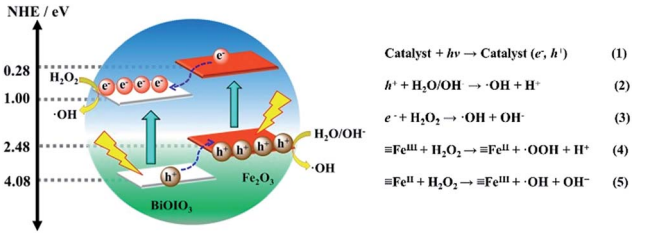

Fig. 7 Pictographic representation and the possible mechanisms involved in the process.

Fe_2O_3/$BiOIO_3$ sample exhibited good photocatalytic activity under irradiation because of the heterojunction structure between $BiOIO_3$ and Fe_2O_3. The photogenerated electrons in the CB (~0.28 eV) of the Fe_2O_3 [27–29] migrated to the CB (~1.00 eV) of the $BiOIO_3$, while the photogenerated holes in the VB (~4.08 eV) of $BiOIO_3$ (ref. 10–12) moved to the VB (~2.48 eV) of Fe_2O_3. As a result, the photogenerated electrons and holes were spatially isolated, which greatly inhibited their undesirable recombination (eqn (1) in Fig. 7). Then the photogenerated holes directly reacted with H_2O or OH^- and converted it into ·OH (eqn (2)). Meanwhile, H_2O_2 chemisorbed on the catalyst surfaces by hydrogen bonding was favorable to trap electrons to produce ·OH (eqn (3)). Whereas excessive Fe_2O_3 would reduce the activity due to its low efficiency. The 15% Fe_2O_3/$BiOIO_3$ sample may be the most satisfying to these requirements. Thirdly, Fenton-like process can generate hydroxyl free radical, this proposal involves the redox cycle of $Fe^{III} \leftrightarrow Fe^{II}$ on the surface, similar to the process occurred in homogeneous Fenton system[24,38] (eqn (4) and (5)). Thus, the synergistic effect of photocatalysis of x% Fe_2O_3/$BiOIO_3$ semiconductor and Fenton-like catalysis would be responsible for the enhanced hydroxyl free radical yield.

4. Conclusions

A series of Fe_2O_3 modified $BiOIO_3$ photocatalysts were prepared using a simple hydrothermal method. There is a strong cooperative effect of bandgaps between these two components, which makes the apparent band gap decrease greatly from 3.00 eV for pure $BiOIO_3$ to 1.81 eV for 30% Fe_2O_3/$BiOIO_3$. The visible light photocatalytic activity for the oxidative degradation of PNP under visible light could be obviously improved. The enhanced catalytic activities of Fe_2O_3/$BiOIO_3$ samples can mainly be ascribed to three factors: Fe ions acted as a mediator of the interfacial charge transfer, the heterojunction structure between $BiOIO_3$ and Fe_2O_3 greatly improved the efficiency of charge separation, the synergistic effect of Fenton-like catalysis. After consecutive catalytic procedures, the catalyst was still stable without obvious deactivation. Coumarin PL experiment confirmed that ·OH was the dominating active species of oxidation process. As a kind of heterogeneous Fenton-like photocatalyst, the Fe_2O_3/$BiOIO_3$ heterojunction is a promising alternative semiconductor for efficient removal of organic pollutants from water.

Acknowledgements

This work was financially supported by the Fundamental Research Funds for the Central Universities (20720170030), and the Educational Commission of XinJiang (XJEDU2014S066). We thank all the graduate students for their assistance with the fieldwork.

References

1 L. Cademartiri, R. Malakooti, P. G. O'Brien, A. Migliori, S. Petrov, N. P. Kherani and G. A. Ozin, *Angew. Chem., Int. Ed.*, 2008, **47**, 3814–3817.
2 X. F. Cao, L. Zhang, X. T. Chen and Z. L. Xue, *CrystEngComm*, 2011, **13**, 1939–1945.
3 L. Zhao, X. Zhang, C. Fan, Z. Liang and P. Han, *Phys. Rev. B: Condens. Matter Mater. Phys.*, 2012, **407**, 3364–3370.
4 H. Li, Y. Cui and W. Hong, *Appl. Surf. Sci.*, 2013, **264**, 581–588.
5 K. Zhao, L. Zhang, J. Wang, Q. Li, W. He and J. J. Yin, *J. Am. Chem. Soc.*, 2013, **135**, 15750–15753.
6 X. Zhang, C. Y. Wang, L. W. Wang, G. X. Huang, W. K. Wang and H. Q. Yu, *Sci. Rep.*, 2016, **6**, 22800.
7 J. Jiang, K. Zhao, X. Xiao and L. Zhang, *J. Am. Chem. Soc.*, 2012, **134**, 4473–4476.
8 J. Jiang, L. Zhang, H. Li, W. He and J. J. Yin, *Nanoscale*, 2013, **5**, 10573–10581.
9 H. Huang, S. Wang, N. Tian and Y. Zhang, *RSC Adv.*, 2014, **4**, 5561–5567.
10 S. D. Nguyen, J. Yeon, S. H. Kim and P. S. Halasyamani, *J. Am. Chem. Soc.*, 2011, **133**, 12422–12425.
11 W. Wang, B. Huang, X. Ma, Z. Wang, X. Qin, X. Zhang and Y. Dai, *Chem.–Eur. J.*, 2013, **19**, 14777–14780.
12 X. M. Qi, M. L. Gu, X. Y. Zhu, J. Wu, H. M. Long, K. He and Q. Wu, *Chem. Eng. J.*, 2016, **285**, 11–19.
13 W. Wang, H. Cheng, B. Huang, X. Liu, X. Qin, X. Zhang and Y. Dai, *J. Colloid Interface Sci.*, 2015, **442**, 97–102.
14 T. Xiong, F. Dong, Y. Zhou, M. Fu and W. K. Ho, *J. Colloid Interface Sci.*, 2015, **447**, 16–24.
15 T. Xiong, H. Zhang, Y. Zhang and F. Dong, *Chin. J. Catal.*, 2015, **36**, 2155–2163.
16 H. Huang, K. Xiao, K. Liu, S. Yu and Y. Zhang, *Cryst. Growth Des.*, 2016, **16**, 221–228.
17 B. Pare, B. Sarwan and S. B. Jonnalagadda, *Appl. Surf. Sci.*, 2011, **258**, 247–253.
18 Z. Liu, B. Wu, Y. Zhu, D. Yin and L. Wang, *Catal. Lett.*, 2012, **142**, 1489–1497.
19 L.-Z. Zhang, H. Chen, X.-F. Zhao, Q. Zhai, D.-J. Yin, Y.-F. Sun and J.-H. Li, *Appl. Catal., B*, 2016, **193**, 47–57.
20 H. Chen, L.-Z. Zhang, H.-H. Zeng, D.-J. Yin, Q. Zhai, X.-F. Zhao and J.-H. Li, *J. Mol. Catal. A: Chem.*, 2015, **406**, 72–77.
21 C. M. Rui, A. F. Rossi and R. M. Quinta-Ferreira, *J. Hazard. Mater.*, 2010, **180**, 716–721.
22 C. M. Rui, D. V. Lopes, M. J. Quina and R. M. Quinta-Ferreira, *Chem. Eng. J.*, 2012, **192**, 219–225.
23 F. Duarte, F. J. Maldonado-Hódar and L. M. Madeira, *Appl. Catal., B*, 2013, **129**, 264–272.
24 L. Xu and J. Wang, *Appl. Catal., B*, 2012, **123–124**, 117–126.
25 N. Wang, L. Zhu, M. Lei, Y. She, M. Cao and H. Tang, *ACS Catal.*, 2011, **1**, 1193–1202.
26 Q. Zhai, L.-Z. Zhang, X.-F. Zhao, H. Chen, D.-J. Yin and J.-H. Li, *Appl. Surf. Sci.*, 2016, **377**, 17–22.
27 M. B. Sassin, A. N. Mansour, K. A. Pettigrew, D. R. Rolison and J. W. Long, *ACS Nano*, 2010, **4**, 4505–4514.
28 P. L. Lee, Y. K. Chiu, Y. C. Sun and Y. C. Ling, *Carbon*, 2010, **48**, 1397–1404.
29 L. L. Peng, T. F. Xie, Y. C. Lu, H. M. Fan and D. J. Wang, *Phys. Chem. Chem. Phys.*, 2010, **12**, 8033–8041.
30 J. Zhu, F. Chen, J. Zhang, H. Chen and M. Anpo, *J. Photochem. Photobiol., A*, 2006, **180**, 196–204.
31 Z. Tao, Y. Li, J. Jing, F. S. Wong and X. Lu, *Sep. Purif. Technol.*, 2008, **62**, 551–558.
32 L. Xu and J. Wang, *J. Hazard. Mater.*, 2011, **186**, 256–264.
33 Q. Liao, J. Sun and L. Gao, *Colloids Surf., A*, 2009, **345**, 95–100.
34 N. K. Daud and B. H. Hameed, *J. Hazard. Mater.*, 2010, **176**, 1118–1121.
35 T. A. Gad-Allah, M. E. M. Ali and M. I. Badawy, *J. Hazard. Mater.*, 2011, **186**, 751–755.
36 S. Guo, X. Li, H. Wang, F. Dong and Z. Wu, *J. Colloid Interface Sci.*, 2012, **369**, 373–380.
37 W. Choi, A. Termin and M. R. Hoffmann, *J. Phys. Chem.*, 1994, **98**, 13669–13679.
38 Y. Gao, H. Gan, G. Zhang and Y. Guo, *Chem. Eng. J.*, 2013, **217**, 221–230.

